Available online at www.sciencedirect.com

ScienceDirect

http://www.elsevier.com/locate/biombioe

Modeling particle population balances in fluidized-bed wood gasifiers

Giovanniantonio Natale [a,1], Antonio Galgano [b], Colomba Di Blasi [a,*]

[a] Dipartimento di Ingegneria Chimica, dei Materiali e della Produzione Industriale, Università degli Studi di Napoli "Federico II", P.le V. Tecchio, 80125 Napoli, Italy

[b] Istituto di Ricerche sulla Combustione, C.N.R., P.le V. Tecchio, 80125 Napoli, Italy

ARTICLE INFO

Article history:
Received 7 August 2012
Received in revised form
19 November 2013
Accepted 10 January 2014
Available online 8 February 2014

Keywords:
Wood
Gasification
Fluidized-bed
Modeling
Particle population balance

ABSTRACT

An unsteady model is developed for the particle size distribution in fluidized-bed reactors including fragmentation, abrasion, elutriation and the chemical reactions of wood gasification. Based on the assumption of constant conditions (gas composition, temperature, velocity) of the surrounding atmosphere, an analytical solution is developed for the distribution of sizes belonging to the classes of mother and fine particles. It is found that for the typical feed sizes (minimum above 3×10^{-2} mm) and the usual maximum size of fine particles (2.4×10^{-3} mm), the behavior of fine particles is quasi-steady with respect to mother particles. The numerical solution of the quasi-steady formulation of particle population balances is also coupled with a two-phase (bubble and emulsion), three-zone (bed, splash zone and freeboard) model for a bubbling fluidized-bed reactor, giving predictions of the producer gas composition in agreement with measurements for air gasification of wood.

1. Introduction

Biomass is the only widespread source of renewable energy and carbon. Increased use of this fuel can contribute in reducing carbon dioxide emissions and enhance energy security. Thermo-chemical conversion has attracted significant interest, in particular gasification, as homogeneous, gas phase combustion of syngas can be more efficient and easier to control than solid fuel combustion. Fluidized-bed gasifiers present the advantages of good temperature control, low-medium tar yields, toleration of variation in the feed quality/size, partial load operation, easy start-up and shut-down and high conversion efficiency although the particulate content in the gas and the carbon loss with ash are higher than for fixed-bed reactors [1]. As pointed out in Ref. [2], the implementation of commercial plant technology traditionally foresees comprehensive experimental investigation, progressing from laboratory scale test units to a pilot-scale plant, before a commercial demonstration plant can be built. In order to optimize the process, extensive experimentation is required for the various scales about the effects of operating and design parameters. This optimization procedure can be speeded up and become less expensive with the aid of mathematical models, on condition that the equation formulation includes all the important chemical and physical processes by describing their mutual interactions and the dependence on the process parameters.

* *Corresponding author*. Tel.: +39 081 7682232; fax: +39 081 2391800.
E-mail address: diblasi@unina.it (C. Di Blasi).
[1] Present address: Department of Chemical Engineering, École Polytechnique, Montreal, Quebec H3C 3A7, Canada.

0961-9534/$ – see front matter © 2014 Elsevier Ltd. All rights reserved.
http://dx.doi.org/10.1016/j.biombioe.2014.01.006

Several transport models have appeared [3–12] for biomass gasification in bubbling fluidized beds, which couple the well known two-phase hydrodynamics with global kinetics, mass and, in a few cases, heat transfer. However, none of them takes into account the distribution of bed particles (particle population). This affects and is, in its turn, affected by the bed hydrodynamics, the extent of chemical reactions, attrition, elutriation and the heat and mass transfer rates.

A great effort has been made in the formulation and solution of particle population balances essentially in the field of coal conversion [13–19] with the exception of Khan et al. [20,21] who consider a fluidized-bed biomass combustor, but a comprehensive unsteady model is still lacking. The models currently available are for a large part for steady-state conditions [13,14,16–18,20,21] using several simplifying assumptions. The unsteady models are based on either an analytical solution [19] or a numerical solution by means of the orthogonal collocation method [15] but attrition of the particles is never taken into account for char, although the treatment proposed for other materials, such as limestone [22], could be extended to the problem under study.

Two main mechanisms of size reduction for carbonaceous particles in fluidized beds are reported [23]: abrasion, where particles of much smaller size break away from the original particle, so that particles become slightly smaller than the original ones, and fragmentation, where the breaking-away process gives rise to a number of particles of smaller size than the original ones. Biomass particles and, in a special way, char particles, generated from the pyrolysis stage, undergo size reduction not only as a consequence of the reactions but also owing to fragmentation and abrasion. The attrited fines can be easily elutriated away unreacted, reducing the process efficiency. For instance, it is pointed out [17] that if a combustor is optimally designed or operated, each 1% efficiency improvement would mean a tremendous cost saving for a power plant.

This study consists of two main parts. In the first part, a comprehensive unsteady model of particle population balance in fluidized-bed gasifiers is proposed. The particle distribution is divided into two size ranges: the class of fine particles contiguous to the class of mother particles. This approach is supported by a number of previous studies [17,18,20,21] and is justified by the fact that there are no significant amounts of intermediate-sized particles between the mother particles and the fines produced from the former by abrasion. Based on the assumption of constant conditions of the surrounding gas, analytical solutions are developed of the model equations for the two size ranges which are used for a parametric analysis with the scope of identifying the processes/parameters which play a controlling role. Also, the conditions are determined which permit a quasi-steady approximation for the behavior of fine particles with respect to the class of mother particles. In the second part of the study, using the analytical solution as a benchmark, a numerical solution is implemented of the quasi-steady version of the model. This is incorporated in a state-of-the-art model for an isothermal bubbling fluidized bed biomass gasifier schematized according to the two-phase theory of fluidization. The coupled particle population balance and the fluidized bed models are used to simulate gasification of wood with air at a laboratory scale obtaining good agreement between measured and predicted gas composition.

2. Mathematical model

The unsteady, one-dimensional mathematical model for the bubbling fluidized bed is formulated in accordance with the two phase theory of fluidization [24], with the existence of an emulsion and a bubble phase, and introducing three spatial zones corresponding to bed, splash zone and freeboard, which are isothermal. The gasifying agent is injected from the bottom while the biomass particles are fed at a certain bed height. The gas phase behaves according to the ideal gas law and is at a constant pressure. The emulsion phase, consisting of an interstitial gas phase at the conditions of minimum fluidization and a solid phase, is assumed to be perfectly mixed. The fuel particles do not contribute in the definition of the void fraction and solid mass of the emulsion phase, given that they are only a small percentage compared with the inert particles. However, their size distribution (and mass) is determined by means of a population balance. The bubble phase consists of gas only and is described by a plug-flow approximation.

A plug-flow approximation is used for the splash and freeboard zones. These, in addition to the gas phase, foresee the presence of a solid phase due to char particle elutriation from the emulsion phase: the particle size is constant and equal to the average value over the size range of the elutriated particles. Also, given the small quantity of solid particles, a unit void fraction and a velocity of the solid coincident with that of the gas are assumed.

2.1. *Chemical reactions and moisture evaporation*

Biomass pyrolysis gives rise to a huge number of chemical compounds which, for engineering applications, are often lumped into three groups: permanent gases, tar and char. They result from both primary decomposition of the solid fuel and secondary reactions of vapor-phase organic products into low-molecular weight gases and char, as they are transported through the particle and the reaction environment. The kinetics of biomass pyrolysis has been extensively investigated [25] but, as the characteristic times are shorter by several order of magnitude with respect to those of the heterogeneous reactions of char conversion [26], the process is often assumed to occur instantaneously. This assumption is retained here, approximating primary degradation of wood by means of a global reaction:

$$\mathrm{Wood} \rightarrow \nu_{\mathrm{C}}\mathrm{Char} + \nu_{\mathrm{CO}}\mathrm{CO} + \nu_{\mathrm{CO_2}}\mathrm{CO_2} + \nu_{\mathrm{H_2}}\mathrm{H_2} + \nu_{\mathrm{CH_4}}\mathrm{CH_4} + \nu_{\mathrm{H_2O}}\mathrm{H_2O} + \nu_{\mathrm{T1}}\mathrm{T_1} \quad \text{(a1)}$$

where the gaseous species, water vapor, primary tar (T_1) and char (Char) are formed with assigned stoichiometric coefficients. The stoichiometric coefficients ($\nu_{CO} = 0.035$, $\nu_{CO2} = 0.035$, $\nu_{CH4} = 0.015$, $\nu_{H2O} = 0.20$, $\nu_{H2} = 0.0015$, $\nu_{C} = 0.215$, $\nu_{T1} = 0.50$) are those corresponding to the yields (%, wt) obtained from the pyrolysis of wood carried out in fluidized beds at temperatures around 800 K [26]. Instead, the thermal

cracking of primary tar, to give gaseous species, water and refractory tar (T_2), occurs with a finite rate:

$$T_1 \xrightarrow{k_{a2}} \nu^*_{CO}CO + \nu^*_{CO_2}CO_2 + \nu^*_{H_2O}H_2O + \nu^*_{CH_4}CH_4 + \nu^*_{H_2}CH_2 + \nu_{T_2}T_2 \quad (a2)$$

$$r_{a2} = A_{a2}\exp\left(-\frac{E_{a2}}{R_gT}\right)\rho_{T_1} \quad (1)$$

again with assigned values for the stoichiometric coefficients. The selected tar cracking kinetics is that reported in Ref. [27]. The stoichiometric coefficients are derived from Ref. [28] with some modifications. It is assumed that a single fraction of primary tar is formed. Moreover the yield of refractory tar (5.8%) is derived from [29], so that the exceeding fraction with respect to the figure given in Ref. [28] (17.5%) is re-distributed over CH_4, H_2 and H_2O. This treatment produces the following values for the stoichiometric coefficients: $\nu^*_{CO} = 0.46$, $\nu^*_{CO2} = 0.08$, $\nu^*_{CH4} = 0.157$, $\nu^*_{H2O} = 0.23$, $\nu^*_{H2} = 0.015$, $\nu_{T2} = 0.058$.

Moisture evaporation is a low temperature process and again, given its short characteristic times compared with those of biomass pyrolysis and char conversion, is assumed to occur instantaneously at the feeding point.

Char particles experience the heterogeneous reactions of combustion and gasification by means of carbon dioxide and steam:

$$CH_\alpha O_\beta + \gamma O_2 \xrightarrow{k_{b1}} \left(2-2\gamma-\beta+\frac{\alpha}{2}\right)CO + \left(2\gamma+\beta-\frac{\alpha}{2}-1\right)CO_2 + \frac{\alpha}{2}H_2O \quad (b1)$$

$$CH_\alpha O_\beta + CO_2 \xrightarrow{k_{b2}} 2CO + \beta H_2O + \left(\frac{\alpha}{2}-\beta\right)H_2 \quad (b2)$$

$$CH_\alpha O_\beta + (1-\beta)H_2O \xrightarrow{k_{b3}} CO + \left(1-\beta+\frac{\alpha}{2}\right)H_2 \quad (b3)$$

The elemental composition of char consists of 95% C, 2% H and 3% O ($\alpha = 0.2526$, $\beta = 0.0237$) [30,31] and the char/oxygen reaction produces a ratio $CO/CO_2 = 0.5$ ($\gamma = 0.8013$).

Some considerations should be made in relation to the selection of the conversion model for the char particles. The approximation of reacting particle (small Thiele numbers, regime I) is never achieved for practical conversion conditions [26]. In this case, based on the evaluation of the Thiele number, it is likely that combustion mainly takes place at the surface (regime III, shrinking particle) while gasification is confined to a surface layer (regime II, variations in both size and density of the particle) [26]. When dealing with reactor models, the description of single particle effects is always based on simplified treatments which, apart from a very few exceptions (for instance a combination of regime I for gasification and regime III for combustion [32]), uses the shrinking particle model (regime III) (for instance [4,7–9,20,21,30,31,33,34]) in some way assuming that the surface layer, where gasification reactions take place, is much smaller than the particle size so that all the reactions can be lumped at the surface. On the other hand, it should also be noticed that population balances, based on particle size distribution, cannot handle the simultaneous variations in space and time of the particle density. Therefore, in this study, single particle effects are again described in accordance with the shrinking particle schematization (there is no surrounding ash layer, justified by the small ash contents of biomass fuels). To account for the simultaneous effects of diffusion through the gas film, adjacent the particle, and intrinsic chemical kinetics, an effective reaction rate, r_j, is introduced assuming a linear dependence on the oxidizing/gasifying species concentration [30,31]:

$$r_j = \frac{c_i}{\frac{1}{k_{m,i}}+\frac{\delta_j}{k_j}}\frac{M_c}{\rho_c}, \quad k_j = A_j\exp\left(-\frac{E_j}{R_gT}\right), \quad j = b1, b2, b3; \quad \delta_j = \gamma, 1, (1-\beta); \; i = O_2, CO_2, H_2O \quad (2-3)$$

where as already done in Refs. [7–10,35], the global mass transfer coefficient is described by the Ranz-Marshall correlation [36]:

$$k_{m,i} = \frac{Sh_iD_i}{d_c}, \quad Sh_i = 2 + 0.6Sc_i^{0.33}Re^{0.5}, \quad Sc_i = \frac{\mu_g}{\rho_gD_i}, \quad Re = \frac{\rho_g u_{mf} d_c}{\mu_g} \quad (4-7)$$

The kinetic data for the heterogeneous reactions (b1–b3) are derived from previous literature: combustion [37], steam gasification [38], carbon dioxide gasification [39].

Combustion of volatile products includes the reactions for primary tar and refractory tar (both modeled as hydrocarbon $CH_{1.522}O_{0.0228}$ [40]), with molecular weight equal to 94 [30,31], methane, carbon monoxide and hydrogen:

$$(T_1)\; CH_{1.522}O_{0.0228} + 0.867O_2 \xrightarrow{k_{c1}} CO + 0.761H_2O, \quad CH_4 + 1.5O_2 \xrightarrow{k_{c2}} CO + 2H_2O \quad (c1-c2)$$

$$2CO + O_2 \xrightarrow{k_{c3}} 2CO_2, \quad 2H_2 + O_2 \xrightarrow{k_{c4}} 2H_2O \quad (c3-c4)$$

$$(T_2)\; CH_{1.522}O_{0.0228} + 0.867O_2 \xrightarrow{k_{c5}} CO + 0.761H_2O \quad (c5)$$

The reaction rates are modeled as in Ref. [40], with the simplifications already introduced in Refs. [30,31] (first-order with respect to fuel (c1,c2,c5) and oxygen (c3)):

$$r_j = A_j\exp\left(-\frac{E_j}{R_gT}\right)Tc_ic_{O_2}, \quad j = c1, c2, c5; \quad i = T_1, CH_4, T_2 \quad (8a-8c)$$

$$r_{c3} = A_{c3}\exp\left(-\frac{E_{c3}}{R_gT}\right)c_{CO}c_{O_2}c_{H_2O}^{0.5}, \quad r_{c4} = A_{c4}\exp\left(-\frac{E_{c4}}{R_gT}\right)c_{H_2}c_{O_2} \quad (9-10)$$

The corresponding kinetic constants are derived from Ref. [40] (c1,c2,c5), [41] (c3) and [30,31] (c4). The water gas shift reaction is also modeled:

$$CO + H_2O \xleftrightarrow{k_{wg}} CO_2 + H_2, \quad r_{wg} = k_{wg}\left(c_{CO}c_{H_2O} - \frac{c_{CO_2}c_{H_2}}{K_E}\right) \quad (wg, 11)$$

with finite rate kinetics

$$k_{wg} = A_{wg}\exp\left(-\frac{E_{wg}}{R_gT}\right), \quad K_E = A_E\exp\left(\frac{E_E}{R_gT}\right) \quad (12-13)$$

Different kinetic constants are used for the spatial zones of the reactor to modulate the catalytic action exerted by ashes, depending on their amounts [42]. Thus the kinetics reported in Ref. [43] is used for the emulsion phase and the splash zone, in the latter case corrected by a factor of 0.25 as already assumed

in Ref. [5]. The kinetics reported in Ref. [44], valid in the absence of significant catalysis, is used for the bubble phase and the freeboard (the equilibrium constant in all cases is derived from Ref. [45]).

2.2. Hydrodynamics

The hydrodynamic model is made by semi-empirical correlations for the variables of interest, such as the minimum fluidization velocity, u_{mf}, [46], the bubble diameter, d_b, [47] which also requires the bubble diameter at the top, d_{bm}, [42], and bottom, d_{b0}, [46], of the bed, the single isolated bubble velocity, u_{br}, [48], the volumetric fraction of the bubble phase, ε_b, with the expansion factor B [42] and the bed height, H_B, obtained from a mass balance on the solid phase:

$$\frac{1.75}{\varepsilon_{mf}^3\varphi_I}\left(\frac{d_I u_{mf}\rho_g}{\mu_g}\right)^2+\frac{150(1-\varepsilon_{mf})}{\varepsilon_{mf}^3\varphi_I^2}\left(\frac{d_I u_{mf}\rho_g}{\mu_g}\right)=\frac{d_I^3\rho_g\left(\rho_I-\rho_g\right)g}{\mu_g^2} \quad (14)$$

$$\frac{d_{bm}-d_b}{d_{bm}-d_{b0}}=\exp\left(-0.3\frac{z}{D}\right),$$
$$d_{bm}=\min\left\{0.652\left[\frac{\pi}{4}D^2\left(\overline{u}_0|_{z=H_B}-u_{mf}\right)\right]^{0.4},D\right\} \quad (15-16)$$

$$d_{b0}=2.78\frac{\left(u_0-u_{mf}\right)^2}{g},\quad u_{br}=0.711\sqrt{gd_b},\quad \varepsilon_b=1-\frac{1}{B} \quad (17-19)$$

$$B=1+10.978\frac{\left(\overline{u}_0-u_{mf}\right)^{0.738}\rho_I^{1.006}}{u_{mf}^{0.937}\rho_g^{0.126}},$$
$$W_I=S\rho_I(1-\varepsilon_{mf})\int_0^{H_B}(1-\varepsilon_b)dz \quad (20-21)$$

The mass transfer between the emulsion and the bubble phase, driven by concentration gradients, is described according to Ref. [24] with the introduction of a global coefficient, K_{be}, consisting of the contributions of two series processes related to the exchange between bubble and cloud phase, K_{bc}, and between cloud and emulsion phase, K_{ce}:

$$\frac{1}{K_{be}}=\frac{1}{K_{bc}}+\frac{1}{K_{ce}},\quad K_{bc}=4.5\frac{u_{mf}}{d_b}+5.85\frac{D^{0.5}g^{0.25}}{d_b^{1.25}},$$
$$K_{ce}=6.77\left(\frac{D\varepsilon_{mf}u_{br}}{d_b^3}\right)^{0.5} \quad (22-24)$$

The total mass flow rate is determined by the inlet gas stream, $\rho_g S u_0$, and the vapor/gas stream generated from wood drying and decomposition, $F_0(1-Y_c)$:

$$\rho_g S\overline{u}_0=\rho_{g0}Su_0+F_0(1-Y_c) \quad (25)$$

where Y_c is the char mass fraction on a moist wood basis. Finally, the property equations are derived from Ref. [49] for the gas viscosity and from Ref. [50] for the species diffusivities.

2.3. Particle size distribution

Comprehensive models of single particle pyrolysis are available including the effects of anisotropy, shrinkage and shape [51–55]. However, all the models of particle population balances are based on one-dimensional spherical particles (shape effects can be taken into account by means of an equivalent diameter and a sphericity factor [34]). Moreover char particles preserve the same shape and size of the corresponding wood particles with a proportional decrease in the intrinsic density. These assumptions are also made in this study.

The biomass particles present a fractional size distribution, p_0^*, that should be assigned. More precisely, the lognormal function is selected [19]:

$$p_0^*=\frac{1}{d\sqrt{2\pi}\ln\sigma}\exp\left[-\frac{1}{2}\left(\frac{\ln(d/\mu)}{\ln\sigma}\right)^2\right] \quad (26a)$$

where μ is the mean and σ is the standard deviation. The function is re-normalized over the range of particle sizes, d_f–d_{max}, that is, the actual range of the particles fed, so that it shows a probability of 1:

$$p_0=\frac{p_0^*}{\int_{d_f}^{d_{max}}p_0^*d(d)} \quad (26b)$$

Based on previous findings [17] and following the schematization used in other studies [18,20,21], it can be assumed that two contiguous size classes exist corresponding to particles indicated as mothers and fines. A mother particle can be fragmented and can be consumed by chemical reactions and abrasion until reaching the upper size limit of the fines, d_f, and becomes a fine itself. Thus the two particle size classes correspond to one range from 0 to d_f for the fines and from d_f to the maximum size, d_{max}, of the mother class. The two classes present a continuous distribution of sizes within the respective range.

Once the char particles are formed, they undergo primary fragmentation that modifies the fractional particle size distribution from p_0 to p_0', although the shape remains unchanged:

$$p_0'(d)=K_f^{1/3}p_0\left(K_f^{1/3}d\right) \quad (27)$$

where K_f is a constant taken equal to 2 as previously done for the fuels of interest [20].

Both classes of char particles experience the heterogeneous reactions of combustion and gasification where the density of the particle is constant but the size is shrinking with a rate R' [m/s]:

$$R'=+(r_{b1}+r_{b2}+r_{b3}) \quad (28a)$$

The abrasion rate, R'', of mother particles is described as in Ref. [56]:

$$R''=\frac{K_a}{3}\left(\overline{u}_0-u_{mf}\right) \quad (28b)$$

where the parameter K_a is equal to 3.5×10^{-7}, which is the range $(2–7)\times10^{-7}$ reported for coal chars [18,20], leading to the formation of fines in accordance with an assigned fractional particle size distribution, p_{0F}, [17]:

$$p_{0F}=\frac{60}{d_f}\left(\frac{d}{d_f}\right)^2\left(1-\frac{d}{d_f}\right)^2 \quad (29)$$

Particles can be elutriated with a rate

$$R_i^{el} = K_{el}\frac{SP_i}{W_I}, \quad i = F, M \tag{30}$$

where P_i is the particle size distribution (kg/m) of fines ($i = F$) or mother ($i = M$) particles and K_{el} the elutriation constant. K_{el} [57] essentially depends on the gas velocity, $\overline{u}_0$, and the terminal velocity, u_t:

$$K_{el} = 0.011\rho_c\left(1 - \frac{u_t}{\overline{u}_0}\right) \tag{31}$$

where the terminal velocity u_t is modeled as in Ref. [58]:

$$u_t = \overline{u}_t\left[\frac{\rho_g^2}{\mu_g\left(\rho_c - \rho_g\right)g}\right]^{-1/3}, \quad \overline{u}_t = \left[\frac{18}{\overline{d}^2} + \frac{0.591}{\overline{d}^{0.5}}\right]^{-1}, \quad \overline{d} = d\left[\frac{\rho_g\left(\rho_c - \rho_g\right)g}{\mu_g^2}\right]^{1/3} \tag{32–34}$$

The mathematical model for the particle population consists of two unsteady one-dimensional (particle diameter) partial differential equations that are hyperbolic in character. The balance for the class of the mother particles is expressed in terms of the particle size distribution, P_M, as:

$$\frac{\partial}{\partial t}P_M = F_0 Y_c p_0' - R_M^{el} - \frac{\partial}{\partial d}RP_M + \frac{3RP_M}{d} \tag{35}$$

where the term on the left hand side is the accumulation. The contributions on the right hand side represent, in the order, the feeding rate, the elutriation rate, the convective term accounting for the displacement from larger to smaller sizes (owing to chemical reactions and abrasion) and the cumulative term for the chemical reaction and the abrasion rates. More precisely, R is the result of the contribution produced by chemical reactions (Eq. (28a)) and abrasion (Eq. (28b)):

$$R = R' + R'' \tag{36}$$

Initially the variable P_M is assumed to be null over the entire range of the mother size class and the boundary condition states that there are no particles at the maximum size, d_{max}:

$$P_M(0, d) = 0, \quad P_M(t, d_{max}) = 0 \tag{37–38}$$

The second partial differential equation is written for the class of fine particles in terms of the particle size distribution, P_F, as:

$$\frac{\partial}{\partial t}P_F = p_{0F}\int_{d_f}^{d_{max}} P_M R_d'' d(d) - R_F^{el} - \frac{\partial}{\partial d}R'P_F + \frac{3R'P_F}{d} \tag{39}$$

The term on the left hand side is again the accumulation. At the right hand side, the various contributions, in the order, represent the production term resulting from the abrasion of the mother particles, the elutriation rate, the convective term taking into account the displacement from larger to smaller sizes, and the reaction rate. The production, due to mother particle abrasion, is expressed as the product of the total mass generated from abrasion and the resulting particle size distribution which is assigned according to Eq. (29). The elutriation rate is again expressed by Eq. (30) while the reaction rate takes into account the contributions of combustion and gasification (Eq. (28a)). The initial conditions again foresee a null distribution while the boundary condition requires the continuity between the two particle classes:

$$P_F(0, d) = 0, \quad P_F(t, d_f) = P_M(t, d_f) \tag{40–41}$$

2.4. Mass conservation equations for the emulsion phase

The model equations for the perfectly mixed emulsion phase consist of the total mass conservation (42) with the reaction term (43) and the definition of the gas volume (44), the conservation of single gaseous species (45a–h), the state equation (46), the definition of the gas density (47), and the mass of char particles for the mother and fine classes (48a–b) (the temperature is referred to the bed value):

$$V_e\frac{d}{dt}\rho_g^e = Su_{mf}\left(\rho_{Air} - \rho_g^e\right) + \sum_i\int_0^{H_B} K_{be,i}\varepsilon_b\left(c_i^e - c_i^b\right)M_i dz + F_0(1 - Y_c) + \sum_{k=1}^{3} R_{et,k}^e - \Delta F^* \tag{42}$$

$$R_{et,k} = \int_{d_f}^{d_{max}} r_k^e\frac{6}{d}\frac{P_M}{\rho_c}M_c d(d) + \int_0^{d_f} r_k^e\frac{6}{d}\frac{P_F}{\rho_c}M_c d(d) \tag{43}$$

$$V_e = S\varepsilon_{mf}\int_0^{H_B}(1 - \varepsilon_b)dz \tag{44}$$

$$V_e\frac{d}{dt}c_i^e = \frac{F_0 Y_{i0}}{M_i} + Su_{mf}\left(c_i^0 - c_i^e\right) + \sum_{k=1}^{3}\nu_{i,k}\frac{R_{et,k}}{M_c} + V_e\sum_{k=4}^{10}\nu_{i,k}r_k^e + \int_0^{H_B} K_{be,i}\varepsilon_b\left(c_i^e - c_i^b\right)dz - \Delta F_i, \quad i = O_2, CO, CO_2, H_2, H_2O, CH_4, T_1, T_2 \tag{45a–45h}$$

$$c_{N_2}^e = \frac{\prod}{RT} - \sum_i c_i^e, \quad \rho_g^e = \sum_i c_i^e M_i \tag{46–47}$$

$$W_M = \int_{d_f}^{d_{max}} P_M d(d), \quad W_F = \int_0^{d_f} P_F d(d) \tag{48a–48b}$$

In addition to the mass exchange between emulsion and bubble phase, originated from the differences in species concentrations and already taken into account through the global coefficient K_{be}, the net flow, ΔF, [42] is also modeled. This is due to variations in the gaseous mass of the emulsion phase to guarantee a constant velocity, equal to the minimum fluidization velocity, following the generation of volatile species from wood drying and decomposition and is expressed as:

$$\Delta F_i = \Delta F^*\frac{c_i^e}{\rho_g^e} \quad \Delta F^* > 0 \tag{49}$$

The set of Eqs. (42,45a–45h) requires assigned initial conditions.

2.5. Mass conservation equations for the bubble phase

The model equations for the one-dimensional, plug-flow bubble phase consist of the total mass conservation (50), the conservation of single gaseous species (51a–51h), the state Eq. (52) and the definition of the gas density (53) (the temperature is referred to the bed value):

$$\frac{\partial}{\partial t}\left(\varepsilon_b \rho_g^b\right) = -\frac{\partial}{\partial z}\left(\varepsilon_b u_b \rho_g^b\right) + \sum_i K_{be,i}\varepsilon_b\left(C_i^e - C_i^b\right)M_i + \frac{\Delta F^*}{SH_B} \tag{50}$$

$$\frac{\partial}{\partial t}\left(\varepsilon_b c_i^b\right) = -\frac{\partial}{\partial z}\left(\varepsilon_b u_b c_i^b\right) + \sum_{k=4}^{10}\nu_{i,k} r_k^b \varepsilon_b + K_{be,i}\varepsilon_b\left(c_i^e - c_i^b\right) + \frac{\Delta F_i}{SH_B},$$
$$i = O_2, CO, CO_2, H_2, H_2O, CH_4, T_1, T_2 \tag{51a–51h}$$

$$c_{N_2}^b = \frac{\prod}{RT} - \sum_i c_i^b, \quad \rho_g^b = \sum_i c_i^b M_i \tag{52–53}$$

with assigned initial conditions. The boundary conditions correspond to known values of the inlet mass fluxes (at $z = 0$).

2.6. Mass conservation equations for the splash and freeboard zones

The model equations for the one-dimensional, plug-flow splash and freeboard zones, with variable cross section $S_{SF}(z)$, consist of the total mass conservation (54), the conservation of single gaseous species (55a–55h), the state equation (56), the definition of the gas density (57) and the mass conservation equation for char (58) with average size of the char particles (59) (the temperature is referred to the bed or the freeboard value):

$$\frac{\partial}{\partial t}\rho_g^{SF} = -\frac{1}{S_{SF}}\frac{\partial}{\partial z}\left(S_{SF} u_{SF} \rho_g^{SF}\right) + \sum_{k=1}^{3}\nu_{c,k} r_k^{SF}\frac{6}{d_{SF}}\frac{\rho_c^{SF}}{\rho_c}M_c \tag{54}$$

$$\frac{\partial}{\partial t}\left(c_i^{SF}\right) = -\frac{1}{S_{SF}}\frac{\partial}{\partial z}\left(S_{SF} u_{SF} c_i^{SF}\right) + \sum_{k=1}^{3}\nu_{i,k} r_k^{SF}\frac{6}{d_{SF}}\frac{\rho_c^{SF}}{\rho_c} + \sum_{k=4}^{10}\nu_{i,k} r_k^{SF},$$
$$i = O_2, CO, CO_2, H_2, H_2O, CH_4, T_1, T_2 \tag{55a–55h}$$

$$c_{N_2}^{SF} = \frac{\prod}{RT} - \sum_i c_i^{SF}, \quad \rho_g^{SF} = \sum_i c_i^{SF} M_i \tag{56–57}$$

$$\frac{\partial}{\partial t}\rho_c^{SF} = -\frac{1}{S_{SF}}\frac{\partial}{\partial z}\left(S_{SF} u_{SF} \rho_c^{SF}\right) - \sum_{k=1}^{3}\nu_{c,k} r_k^{SF}\frac{6}{d_{SF}}\frac{\rho_c^{SF}}{\rho_c}M_c \tag{58}$$

$$\overline{d}_{SF} = \frac{\int_{d_f}^{d_{max}} R_M^{el} d(d) + \int_0^{d_f} R_F^{el} d(d)}{\int_{d_f}^{d_{max}} \frac{R_M^{el}}{d} d(d) + \int_0^{d_f} \frac{R_F^{el}}{d} d(d)} \tag{59}$$

Boundary conditions, at the bottom of each zone, require the continuity of the mass fluxes taking into account that char particle transport occurs via elutriation.

3. Analytical solutions of the particle population balances

To develop an analytical solution of the model equations for particle size distribution, in the first approximation, it is assumed that the conditions of the surrounding gas (velocity, temperature and species concentration) are assigned at constant values, so that reaction, abrasion and elutriation rates are also constant. The analytical solution is developed with the same approach detailed in Ref. [19], although significant differences exist between the two mathematical models. Therefore modifications are introduced in the solution procedure in order to take correctly into account the new features. In this study two size classes of particles are considered versus the single class used in Ref. [19]. Hence the solutions should be determined for two partial differential equations (Eqs. (35) and (39)), which are coupled through the time-dependent boundary condition (Eq. (41)), instead of the simpler constant value at the boundary imposed in the previous work. Moreover, the present treatment introduces some additional features: a) a more realistic description of the heterogeneous reaction rates is used (Eqs. (2) and (3)) instead of a the simple expression $A'/(d + B')$, where A' and B' are assigned constants, b) the effects of attrition are taken into account and c) a more general treatment of the elutriation process is proposed instead of a simple on/off process where all fuel particles smaller than a critical size are elutriated whereas the larger particles remain in the system.

The following expressions are obtained for P_M and P_F:

$$P_M(d,t) = -F_0 Y_c \frac{d^3}{R}\int_d^{d_{max}} \frac{p'_0}{d'^3} u\left(t + \int_d^{d'}\frac{1}{R}d(d)\right)\exp\left(\int_d^{d'}\frac{K_{el}S}{W_I R}d(d)\right)d(d') \tag{60}$$

$$P_F(d,t) = P_{F1}(d,t) + P_{F2}(d,t) \tag{61}$$

$$P_{F1}(d,t) = -\frac{d^3}{R'(d)}\int_d^{d_f}\frac{p_{0F}}{d'^3}u\left(t + \int_d^{d}\frac{1}{R'}d(d)\right)\dot{m}_F\left(t + \int_d^{d}\frac{1}{R'}d(d)\right)$$
$$\times\exp\left(\int_d^{d'}\frac{K_{el}S}{W_I R'}d(d)\right)d(d') \tag{62a}$$

$$P_{F2}(d,t) = -\left(\frac{d}{d_f}\right)^3\frac{R'(d_f)}{R'(d)}P_M(d_f,t)\exp\left(\int_0^{d_f}\frac{K_{el}S}{W_I R'}d(d)\right) \tag{62b}$$

where $\dot{m}_F(t)$ represents the mass flux of fines produced by abrasion of mother particles according to the following equation (Eq. (63)):

$$\dot{m}_F(t) = \int_{d_f}^{d_{max}} P_M R''_d d(d) \tag{63}$$

Eqs. (60)–(62) provide the following steady-state distributions for $t \to \infty$:

$$P_M(d) = -F_0 Y_c \frac{d^3}{R} \int_d^{d_{max}} \frac{p'_0}{d'^3} \exp\left(\int_d^{d'} \frac{K_{el} S}{W_I R} d(d) \right) d(d') \quad (64)$$

$$P_F(d) = P_{F1}(d) + P_{F2}(d) \quad (65)$$

$$P_{F1}(d) = -\frac{d^3}{R'(d)} \int_{d_f}^{d_{max}} P_M R''_d d(d) \int_d^{d_f} \frac{p_{0F}}{d'^3} \exp\left(\int_d^{d'} \frac{K_{el} S}{W_I R'} d(d) \right) d(d') \quad (66a)$$

$$P_{F2}(d) = -\left(\frac{d}{d_f}\right)^3 \frac{R'(d_f)}{R'(d)} P_M(d_f) \exp\left(\int_0^{d_f} \frac{K_{el} S}{W_I R'} d(d) \right) \quad (66b)$$

In the problem schematization it is assumed that the mother and fine classes of particles are contiguous. However, it has been demonstrated [17,18,20,21,23] that in fluidized bed reactors attrition essentially occurs by means of an abrasive-type mechanism and thus, between the son particles (a subclass of the mother particles, produced from the fragmentation and abrasion processes) and the fines produced, the range of intermediate-sized particles is almost empty in terms of mass. This circumstance provides the basis for an analysis of the characteristic evolution times for the two size classes introduced which, given the large size differences, are expected to show highly different values. Indeed, as discussed in the following, it is found that, for the conditions typical of fluidized-bed gasification, the characteristic times for the fines are several order of magnitude shorter than those of the mothers. Consequently it is reasonable to assume that the class of fine particles exhibits a quasi-steady behavior with respect to the class of mother particles. In this way, the unsteady equation for the population balance for the mother class (Eq. (35)) can be coupled, through the boundary conditions (Eq. (41)), to the steady-state version of the population balance equations of the fines (Eq. (39)) and the solution given by Eq. (60) with that given by Eq. (65). The validity of the quasi-steady approximation will be discussed in relation to the range of typical operating conditions of fluidized-bed gasifers.

4. Numerical solution

The assumption that the environment external to the particles is at uniform and constant conditions in terms of temperature, species concentrations and velocity is no longer valid when the particle population equations are coupled with chemical reactions and the heat and mass transfer processes for the fluidized-bed gasifier. On the other hand, given the complexity of the conservation equations for the latter, a numerical solution should be anyway implemented. A semi-implicit finite-difference procedure is applied here. For each time step, the numerical solution for the population balance equations is carried out first, using the last available values for the variables obtained from the equations for the different zones of the fluidized bed. Then these are solved using the solution already determined for the particle size distribution. The two stages of the solution procedure are repeated for successive time intervals until steady-state conditions are attained.

The numerical solution of the population balance equations is based on the assumption of quasi-steady behavior, that is, the analytical solution (65) of the steady formulation of the equation for the fine particle class is combined with the numerical solution of the unsteady equation (35) for the mother particles. This is based on the operator splitting procedure [59] and finite differences approximations of the convection terms using the Flux-Corrected-Transport (FCT) scheme with reference to the explicit SHASTA phoenical version [60]. The procedure foresees two stages corresponding to convective transport and the remaining contributions at the right hand side of the equation. Thus, for each time step, after convective transport, the ode15s integrator of the Matlab platform is applied. Then, using the last available values for the abrasion rate and the boundary condition (41), the analytical solution (65) is applied for the class of fine particles. In this stage of the computational procedure, the conditions external to the particles are given by the last available values of the solution of the equations for the fluidized-bed reactor.

As for the different spatial zones of the fluidized-bed reactor, the convective terms of the equations for the bubble, the splash and the freeboard zone are discretized by means of the finite difference backward scheme. In this way, each partial differential equation is approximated by a system of N ordinary differential equations (N is the number of spatial cells). A staggered grid is employed where the process variables are positioned at the center of the cell and the velocity at the cell boundaries. The resulting system of ordinary differential equations together with the ordinary differential equations for the emulsion phase and all the algebraic equations are solved using again the ode15 integrator of the platform Matlab. In this stage of the computational procedure, the particle size distribution coincides with the last available.

5. Results

Wood gasification with air in a fluidized bed is studied. The results consist of two main parts. In the first one, the dynamics of particle size distribution are discussed. In the first place, the analytical solutions of the particle population balances are applied to simulate the effects of the composition of the surrounding gas and the feed size. In this way, the conditions which permit the application of the quasi-steady approximation of the fine with respect to the mother class are also determined. In the second part, results are discussed of the simulations of the coupled numerical solution of the particle population balance model with the transport equations for a bubbling fluidized-bed gasifier, providing a comparison between predictions and measurements of the composition of the gas produced at steady-state conditions.

5.1. *Dynamics of particle population*

In this section results are presented about the dynamics of particle size distribution, assuming that the environment external to the particle is at assigned conditions. Typical operating conditions correspond to a fuel feed rate of 0.28 kg s^{-1} with an air (kg) to fuel (kg) ratio of 1.8, a bed temperature of 1073 K and a fluidizing gas velocity of 1 m s^{-1}. The

bed is assumed to consist of silica sand particles (size 500 μm) with a sphericity factor of 0.86. For the reference case, the particle size distribution of the feed is assumed to be comprised (99.5%wt) in the range d_{min}–d_{max} with values of 10 and 30 mm, respectively, whereas the limit diameter, d_f, positioned at the boundary between the classes of mother and fine particles, corresponds to 2.4×10^{-3} mm [20]. The density of the char particles is 125 kg/m^3. Two cases are considered for the chemical composition of the gaseous environment surrounding the particles: A) it is a mixture obtained from the pyrolysis gas and the inlet air (molar composition: $X_{O2} = 0.141$, $X_{N2} = 0.5295$, $X_{CO} = 0.091$, $X_{CO2} = 0.023$, $X_{H2} = 0$, $X_{H2O} = 0.154$, $X_{CH4} = 0.052$, $X_{T1} = 0$, $X_{T2} = 0.0092$) or B) it is the typical gas composition at the exit of a bubbling fluidized-bed gasifier (molar composition: $X_{O2} = 0$, $X_{N2} = 0.36$, $X_{CO} = 0.14$, $X_{CO2} = 0.12$, $X_{H2} = 0.10$, $X_{H2O} = 0.28$, $X_{CH4} = 0.0$, $X_{T1} = 0$, $X_{T2} = 0$). These two atmospheres are indicated in the following as A and B.

Three cases of mass transfer between gas and particles have been identified for fluidized-bed reactors depending on the relative size of the active particles and the bed particles [61]. For particles much smaller than the bed particles it is appropriate to use the Frossling correlation [62]. For particle sizes comparable to the bed particles, the correlation proposed by La Nauze and Young [63] is widely used which, for larger particles, is substituted by the correlation proposed by Prins et al. [64]. Given the range of particle sizes typical of fluidized bed reactors (2–5 mm [65]), the chemical times evaluated with the above correlations for the problem under study show values coincident or only slightly shorter than those obtained by means of the Ranz-Marshall correlation. As already observed, in practical cases, the lower-size part of the mother class is almost empty, which also enhances the actual differences between the characteristic times for the two classes. Based on these considerations, it is important to establish the validity limits of the assumption of a quasi-steady behavior of the fine versus the mother class.

To analyze the dynamics of the particle size distribution, the unsteady analytical solutions (60,61) are applied for the reference case. A grid of 1000 cells, for each of the two particle classes, is used for the numerical evaluation of the integrals (a grid of 100 cells for the fine class introduces deviations on output variables below 3%). The variables P_M and P_F, as computed for the atmosphere A, are shown for several times in Fig. 1A and B. As expected, the examination of the various global rates (the contributions in the conservation equations integrated over the particle size) confirms that for the mother class the dominant process is the chemical reaction rate that, at steady conditions, practically balances the inlet rate of the fragmented char particles. The contributions due to abrasion, convective outflow and elutriation rates are smaller by approximately two, eight and six orders of magnitude, respectively. The main inlet contribution for the fine class is due to the abrasion rate of mother particles which, at steady conditions, is again balanced by the chemical reaction rate (the convective inlet rate and the elutriation rate are smaller by about six orders of magnitude). Both the mass, for a given particle size, and the different global rates continuously increase in time until steady conditions are achieved for times around 260s (corresponding to the attainment of 95% of the total final char bed loadings for the two particle classes). Given the coupling resulting from the convective outflow and the abrasion rate from the mother class to the fine class, the times needed to achieve steady values of the related char bed loading are the same.

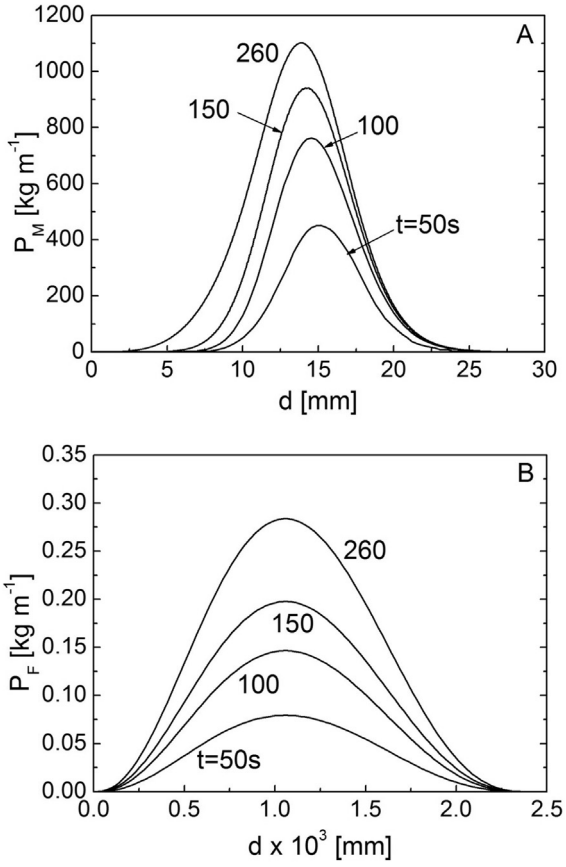

Fig. 1 – Particle size distributions for the mother class, P_M, (A) and the fine class, P_F, (B) for several times and atmosphere A (reference case).

The P_M and P_F curves provide information about the mass of char particles in the bed of a given size. Thus, in general, both the mass and the size range may change in time. Indeed, Fig. 1A shows that, while the mass increases with time, the particle size range for the mother class tends to be displaced towards successively smaller values. This can be better seen from Fig. 2, which shows the corresponding fractional particle size distribution, p_M (that is, P_M referred to the total mass), at steady conditions and the corresponding values for the char feed, p_0, and the fragmented char particles, p_0'. For the mother class the times needed to achieve the steady conditions, in terms of mass and particle size range, are the same and approximately correspond to the characteristic chemical times that, for the sizes of interest, are of the order of hundreds of seconds. Instead, the P_F curves reported in Fig. 1B show that, while the mass continuously increase in time, the size range for the fine class is invariant already at short times. Early process dynamics show that a steady range of particle size for the fine class is attained within times of the order of milliseconds. Again, these times are essentially those of the

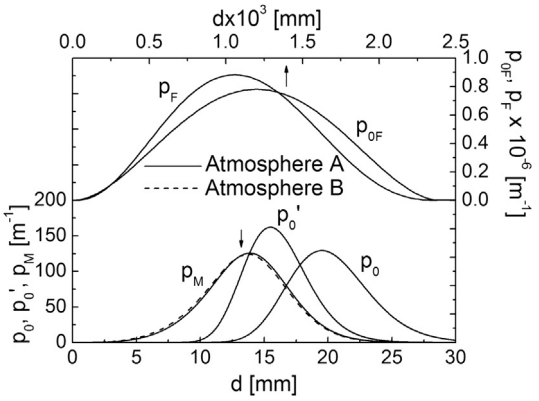

Fig. 2 – Steady-state fractional particle size distributions for the mother class, p_M, and the fine class, p_F, for the atmosphere A (solid line) and atmosphere B (dashed line) and the reference case. For comparison purposes, the fractional particle size distribution of the feed, p_0, and the fragmented particles, p_0', and the abraded particles, p_{0F}, are also included.

chemical reactions. Also, in this case there is a displacement of the particle size range towards lower values as shown by a comparison between the fractional mass size distribution at steady conditions, p_F, and the corresponding value for the fine distribution from abrasion, p_{0F} in Fig. 2. In other words, although inlet and outlet global mass feed rates change over long times, as determined by the characteristic times of the mother particles, given that the size range of inlet particle is constant in time, a steady distribution is achieved within the times required by the chemical reactions to occur. These, being the particle sizes very small, are much shorter than those typically associated with the size evolution of the mother class.

The process dynamics remain qualitatively the same for the atmosphere B and the relative importance of the various contributions in the conservation equation is also left unaltered. The steady fractional mass distributions reported in Fig. 2 indicate that the particle sizes of the mother class are barely displaced towards smaller values whereas for the fines there are no appreciable changes. The curves of the char bed loading versus time (Fig. 3) show that higher values are reached for the atmosphere B (factors of about 1.5 and 8.5 for the mother and fine classes) and that the times needed to achieve steady conditions are also longer (about 360s versus 260s). These features can be explained by observing that the fastest chemical reaction rate for the atmosphere B (steam gasification) presents characteristic times that, for a kinetic or a mixed kinetic-diffusive control, are significantly longer than those of the oxidation rates of atmosphere A. The qualitative features of the particle size distribution remain the same as the gas velocity and the temperature of the surrounding environment are varied (the abrasion and elutriation rate increase as the velocity is increased or the temperature is decreased).

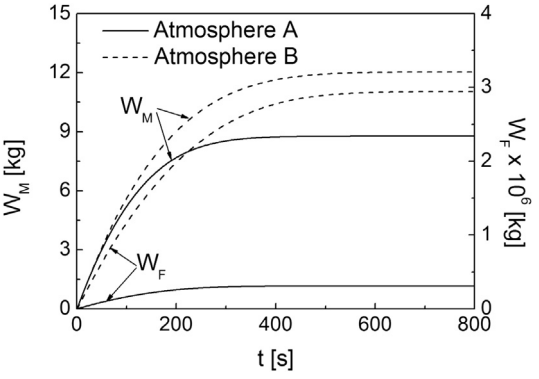

Fig. 3 – Char bed loading versus time for the mother class, W_M, and the fine class, W_F, for the atmosphere A (solid line) and atmosphere B (dashed line) and the reference case.

To further investigate the dynamics of particle size distribution, feed sizes are varied in the ranges d_{min}–d_{max} (99.5%wt) of 25–50, 20–40, 5–20, 1–5 and 0.1–1 mm. A grid consisting of 1000 cells, for each of the particle class, gives accurate computation of the integrals. The qualitative features of the process again remain the same as discussed for the reference case (d_{min}–d_{max} = 10–30 mm). As expected, the time needed to attain steady conditions and the steady char bed loadings show successively lower values as the feed sizes are progressively reduced. The increase in the rate of the heterogeneous reactions of char conversion, the dominant contribution in the particle size population balance, is responsible for such a behavior. Also, the qualitative effects of the reaction environment remain the same as already reported for the reference case. For instance, the time needed to attain steady conditions varies from about 720 to 1 s (atmosphere A) or from about 880 to 6 s (atmosphere B). The steady char bed loading for mother particles is also different with values in the range 24–0.04 kg (atmosphere A) or 29–0.18 kg (B). The times needed to achieve steady conditions for the class of fine particles are the same as for the mother class (the steady char bed loading values also decrease although values are always very small).

Examples of the steady profiles of the fractional particle size distribution for the mother class are plotted in Fig. 4

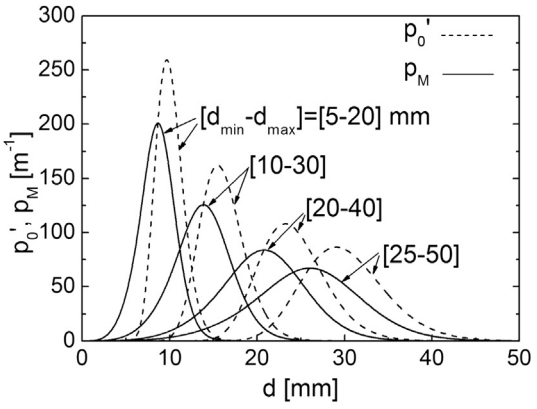

Fig. 4 – Steady-state fractional particle size distributions for the mother class, p_M, for the atmosphere A and various ranges d_{min}–d_{max} of the feed particles (solid line). For comparison purposes, the fractional particle size distributions of the fragmented particles, p_0', are also included (dashed line).

where, for comparison purposes, the initial distribution for the fragmented particles is also shown. The two profiles are similar although, due to chemical reaction and abrasion activity, the percentage of smaller particles for the former increases significantly especially when larger feed particles are considered. Indeed, the maximum p_M is always located in correspondence of the descending zone of the left-hand side of the p_0' distribution and attain a lower value. Obviously, the dominant term, at steady conditions practically balancing the feed rate, is always due to the chemical reaction rate. However, by decreasing the feed size range, at steady conditions, the global elutriation rate and the convection rate increase by about four and two orders of magnitude (atmosphere A) or five and two orders of magnitude (atmosphere B) (information on the steady profile of the elutriation rate distribution can be obtained from Fig. 5, where maximum values are increased up to factors of about 7 (atmosphere A) or 28 (atmosphere B)).The steady abrasion rate decreases by approximately one order of magnitude. It is important observing that, given the constant particle size distribution from the abrasion rate p_{0F}, the steady fractional particle size distribution for the fine particles remains unvaried with respect to the profile reported in Fig. 2. Indeed the chemical reaction rate again practically balances the abrasion rate for all the feed size ranges investigated. However, as the feed particles are displaced towards smaller values, given the constant distribution in the size of fine particles and the progressive diminution in the char bed loading, the elutriation rate decreases, remaining from about six to five orders of magnitude slower (see Fig. 5 for the steady profile of the elutriation rate distribution which shows reductions up to factors of about 9 (atmosphere A) or 3 (atmosphere B)). The steady convective transport rate are also still slower by about six or three orders of magnitude.

Computations of the dynamics of particle size distribution for all the cases examined, which approximately span the typical conditions established in fluidized-bed gasifiers, provide the same results by using either the fully unsteady solutions or the quasi-steady-solutions, indicating that the latter can be safely applied. To further investigate the applicability of this treatment the case is considered of a very small feed size range corresponding to d_{min}–d_{max} = 0.03–0.1 mm, that is, for conditions of a very close coupling between the two size classes (grids with 1000 cells again provide an accurate numerical evaluation of the integrals). Fig. 6A and B summarizes the results in terms of particle size distribution (at several times) and char bed loading profiles for the two classes of particles and the atmosphere A. The steady distribution of the particle size for the mother class is always dictated by a balance between the feed rate and the chemical reaction rate with the elutriation, abrasion and convection rate smaller by about four, three and four orders of magnitude respectively. Given the small particle sizes and the fast rate of heterogeneous conversion, steady conditions are attained within very short times (about 0.1 s). Times needed to achieve steady conditions are longer (by a factor of approximately 2) for the class of fine particles. In this case, the reaction rate is still the most important outlet contribution (the steady elutriation rate is smaller by about six orders of magnitude). However, the inlet rate is represented not only by the abrasion rate of the mother particles but also by the convection term (boundary condition) which, at steady conditions, is smaller only by a factor of about 2.7. In other words, the convection term is negligible for the

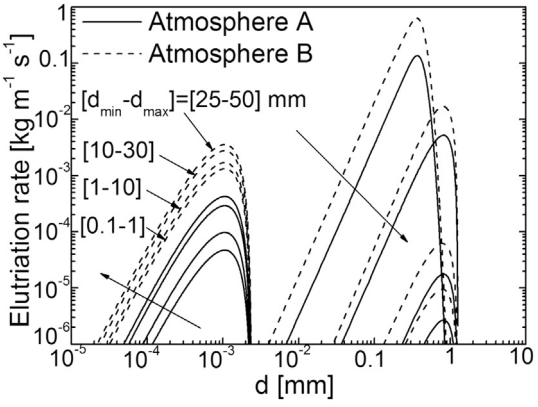

Fig. 5 – Steady distribution of the elutriation rate for the atmosphere A (solid line) and atmosphere B (dashed line) and various ranges d_{min}–d_{max} of the feed particles: the elutriation rate increases and decreases, according to the direction of the main arrows, for the fine and mother classes, respectively.

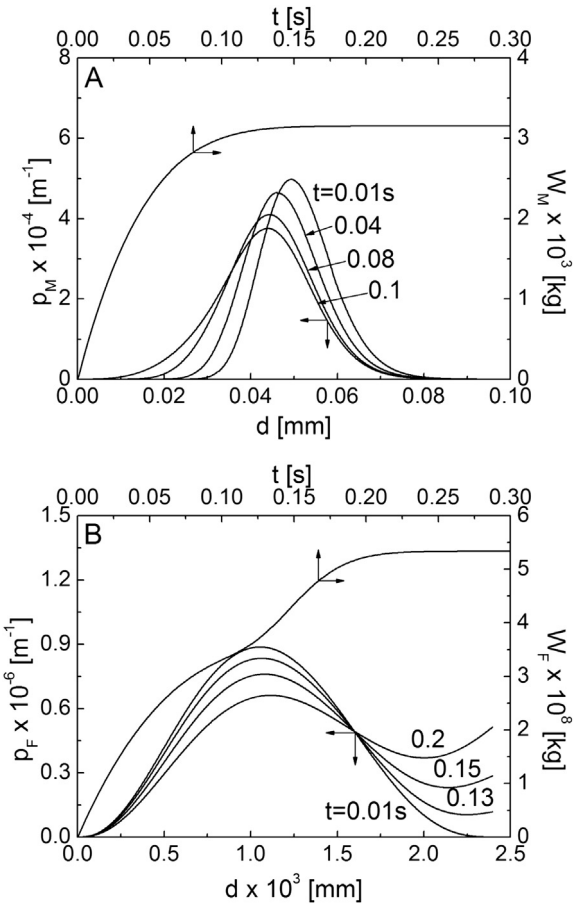

Fig. 6 – Fractional particle size distribution for the mother class, p_M, (A) and fine class, p_F, (B) and corresponding char bed loadings, W_M and W_F, versus time for several times and atmosphere A (feed range d_{min}–d_{max} equal to 0.03 mm–0.1 mm).

Table 1 – Predicted (S) and measured (E) gas composition, as percent on a molar basis, and LHV and tar content of the gas for six tests reported in Ref. [66].

Test number	1		2		3		4		5		6	
F_0 [g s^{-1}]	0.16		0.153		0.108		0.19		0.182		0.188	
Moisture content [%wt]	23.5		21.0		23.0		22.0		25.0		19.0	
ER	0.32		0.37		0.47		0.26		0.36		0.32	
T_B [K]	1073		1073		1083		1073		1063		1073	
T_F [K]	813		823		773		873		833		803	
Carbon conversion [%wt]	84.4		91.2		71.5		76.4		87.3		92.3	
	E	S	E	S	E	S	E	S	E	S	E	S
CO	14.0	**14.4**	13.0	**15.2**	10.0	**10.2**	13.0	**15.8**	13.0	**15.4**	18.0	**17.8**
CO_2	13.5	**14.1**	15.0	**13.6**	12.0	**14.3**	15.0	**13.9**	15.0	**13.2**	13.5	**12.3**
$CH_4 + C_2H_4$	4.2	**4.7**	4.3	**4.6**	3.5	**2.1**	4.3	**5.6**	4.3	**4.2**	6.8	**4.7**
H_2	7.0	**10.0**	9.5	**10.4**	8.0	**4.9**	9.5	**12.0**	9.5	**10.0**	9.5	**11.8**
N_2	61.3	**69.0**	58.3	**56.1**	66.5	**68.4**	58.3	**52.7**	58.3	**57.2**	52.2	**53.3**
H_2O	8.0	**26.1**	7.7	**24.1**	27.0	**26.4**	21.6	**26.5**	24.0	**26.6**	0.24	**23.1**
TAR [g m^{-3}]	3.73	**6.99**	7.16	**7.09**	2.99	**3.17**	2.01	**8.32**	2.01	**6.34**	9.98	**7.36**
LHV [MJ m^{-3}]	4.3	**4.6**	4.6	**4.7**	3.7	**2.6**	4.6	**5.3**	4.6	**4.5**	6.3	**5.2**

population balance of the mother particles but it is important for the fine particles. It increases in time and causes a progressive variation in the shape of the size distribution of fine particles. At very short times this reproduces the same qualitative trends shown in Fig. 1B. However, as the convection rate increases, the mass of particles with sizes displaced towards larger values becomes progressively higher. The time profile of the char bed loading clearly shows that there is a first zone, approximately corresponding to times needed by mother particles to attain steady conditions, essentially determined by the abrasion rate of mother particles and a second period determined by both abrasion and convection rates of mother particles. Similar results are also obtained for the atmosphere B although the time needed to achieve a steady state is longer. For this range of small-sized feed particles the quasi-steady solution over-predicts the particle size distribution of fine class with deviations that are time and size dependent. Maximum deviations, corresponding to about 40%, are observed around the boundary between the fine and the mother class for a time approximately coincident with that of the steady solution of the mother class. Deviations for the smaller sizes are approximately around 10%. In all cases, they tend to decrease as steady conditions for the class of fine particles are approached. Therefore, in the case of a close coupling, the assumption of a quasi-steady behavior of the fine with respect to the mother class cannot be applied.

The analytical solution of the particle population balance has also been applied to evaluate the accuracy of the numerical solution using the reference case. Simulations have been made using 100, 200, 300, 400 and 500 cells with time steps of 0.01 s for Eq. (35). Deviations between the numerical and the analytical solutions, in terms of particle size distribution and char bed loading, at very short times (below 10 s) reach values up to 20–30% that appear to be insensitive to the number of cells. Then deviations on the particle size distribution decrease to values below 1% already for a grid of 300 cells (about 10% for a 100 cell grid). A similar trend is observed for the deviations in the char bed loading which also shows lower values. Thus, apart from the very initial transients, the numerical solution gives accurate predictions already with a relatively coarse grid.

5.2. *Bubbling fluidized bed simulations*

The coupled model for the particle size distribution and the bubbling fluidized bed is applied to simulate the laboratory-scale system developed in Ref. [66]. It is made by a bottom vessel with a height of 0.6 m and diameter of 0.06 m, where the expanded bed and the splash zone are located, and un upper vessel with a height of 0.2 m which also present an increase in the diameter (over a length of 0.05 m) from 0.06 m to 0.12 m, which represents the freeboard zone. The bed material is silica sand (0.5 kg) with sizes between 320 μm and 500 μm. The wood feed rates are approximately in the range 0.1 g s^{-1}–0.2 g s^{-1} with equivalent ratios (ER) between 0.26 and 0.47 (corresponding air (kg) to fuel (kg) ratios of 1.4–2.4), the bed temperatures, T_B, around 1063–1083 K and freeboard temperatures, T_F, around 773–873 K. Pine wood particles sizes are between 0.8 mm and 4 mm and the initial density is 450 kg m^{-3} which, in accordance with the stoichiometry of the pyrolysis reaction, gives rise to a char density of 96.75 kg m^{-3}. The maximum diameter for the class of fine particles, d_f, is again assumed equal to 2.4 × 10^{-3} mm [20]. The carbon

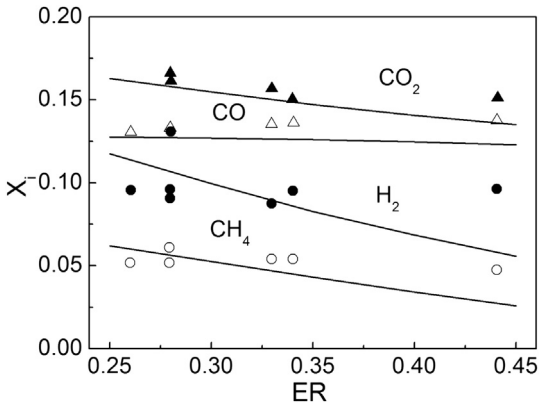

Fig. 7 – Measurements (symbols [66]) and predictions (lines) of the dry gas composition, on a molar basis, versus the equivalent ratio, ER (wood feed rate 0.12 g s^{-1}, moisture content 21% wt, carbon conversion 84% wt, T_B = 1073 K, T_F = 823 K).

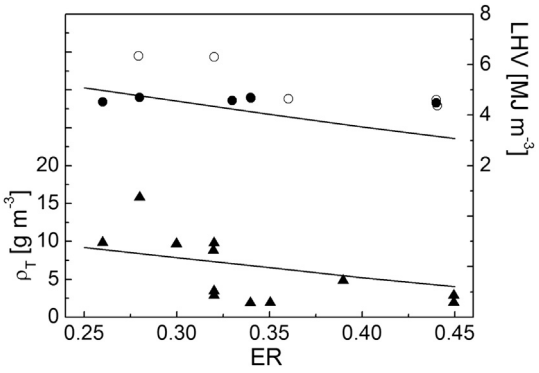

Fig. 8 – Measurements (symbols [66]) and predictions (lines) of the LHV of the gas and the tar content of the gas versus the equivalent ratio, ER (the measured LHV values include those given in Ref. [66] (open symbols) and those evaluated from the gas composition (standard conditions) reported in the same study (full symbols)) (conditions as in Fig. 7).

conversion, evaluated from the elemental composition of wood and the composition of the gas provided for six typical gasification experiments is between 70 and 90%. In the simulations it is assumed that the unconverted carbon belongs to the char product with a corresponding decrease in the feed rate. The initial conditions foresee that the gas phase consists of air at the assigned temperature for the bed and the freeboard. Then wood is fed to the gasifier and the conversion process begins. Feeding takes place in the emulsion phase and the excess gas/tar produced, with respect to the conditions of minimum fluidization, is uniformly distributed across the bubble phase.

Similar to previous models of fluidized-bed gasifiers [4–12], the experimental validation of the model is made considering the composition of the gas, as this is largely dependent on the chemical kinetics and transport phenomena [67]. Indeed, for these gasifiers, the temperature is approximately uniform but rather low. Hence heterogeneous chemical equilibria will usually not be attained and only serve to set the trend of the variations in gas composition with the operating parameters. Homogeneous equilibrium is more likely to be established, as the water gas shift reaction is essentially in equilibrium above 1100 K.

An acceptable agreement between measured and predicted properties of the gas for six typical experiments reported in Ref. [66] is obtained as shown by the data listed in Table 1. It is plausible that there is a misprint in the reported experimental values for the H_2O yields for the experiments N.1 and N.2, as these values are lower by a factor of about three with respect to those of the other experiments and the predictions of the model.

A further comparison between predictions and measurements can be made through Fig. 7 (gas composition, as a percent on a molar dry basis) and Fig. 8 (gas lower heating value (LHV) and tar content of the gas) for ER values in the range 0.25–0.45 (wood feed rate 0.12 g s^{-1}, moisture content 21%, carbon conversion 84%, T_B = 1073 K, T_F = 823 K). As ER is increased, the CO, CO_2, CH_4 and H_2 concentrations decrease as a consequence of the successively higher amounts of nitrogen which prevails upon the effects deriving from an enhanced activity of the combustion reactions which are responsible for the reduction in the tar content of the gas. In general, the model provides good quantitative results although the predictions indicate a stronger dependence of the H_2 concentration on ER. The maximum steady elutriation rate distribution increases with ER with values in the range (1–2) × 10^{-5} kg m^{-1} s^{-1} for the mother class and corresponding values for the fines lower by 5 orders of magnitude.

Acceptable agreement between predictions and measurements of the gas composition is also obtained for various bed temperatures as shown in Fig. 9 for the gas composition and Fig. 10 for the gas LHV and the tar concentration (wood feed rate 0.67 kg/h, moisture content 21%, carbon conversion 84%, ER = 0.3, T_F = 923 K). As the bed temperature is increased, the steam gasification of char becomes more favored with respect to CO_2 gasification (higher activation energy) with an increase in the production of H_2. Moreover, the forward path of the

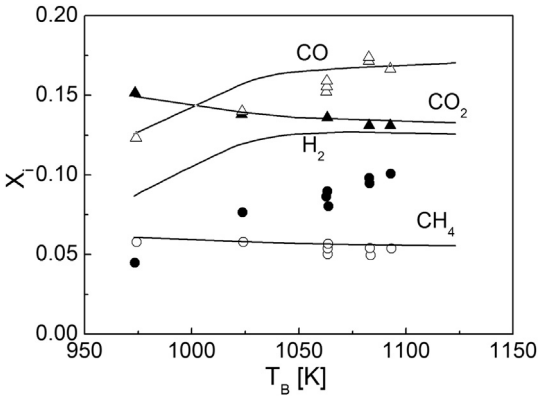

Fig. 9 – Measurements (symbols [66]) and predictions (lines) of the dry gas composition, on a molar basis, versus the bed temperature, T_B (wood feed rate 0.19 g s^{-1}, moisture content 21% wt, carbon conversion 84% wt, ER = 0.3, T_F = 823 K).

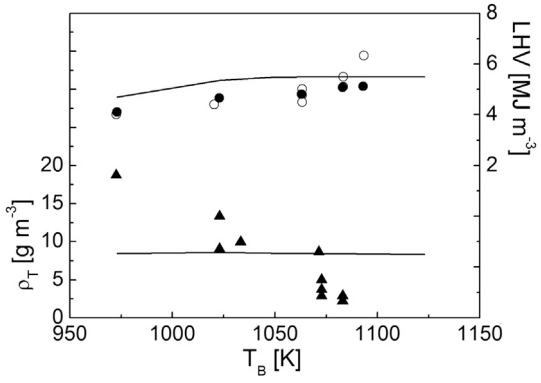

Fig. 10 – Measurements (symbols [66]) and predictions (lines) of the gas LHV and tar content of the gas versus the bed temperature, T_B (the measured LHV values include those given in Ref. [66] (open symbols) and those evaluated from the gas composition (standard conditions) reported in the same study (full symbols)) (conditions as in Fig. 9).

water gas shift reaction becomes less favored, with an increase in the production of CO (and a diminution in the production of CO_2). The CH_4 yields remain approximately constant. The model over-predicts the yields of H_2. However, as observed in Ref. [66], the measured yield of this products vary over a rather wide range that, for the temperatures of interest here, is about 8–14% and is comparable with the values given by the model. Finally, although the predicted tar content of the gas is close to the measured values, the model does not predict the slight decrease as the temperature is increased. This can be attributed to steam reforming that is not included in the reaction network considered here. Again, the elutriation rate distribution decreases as T_B is increased with maximum steady values diminished by one order of magnitude over the range of interest.

6. Conclusions

A comprehensive unsteady model for the distribution of particle sizes in fluidized-bed reactors has been developed including fragmentation, abrasion, elutriation and the chemical reactions of wood gasification. The particle distribution is divided into two size ranges: the class of fine particles contiguous to the class of mother particles. Simulations, carried out by varying temperature, composition and velocity of the surrounding gas and feed size range over conditions that span those typically established in fluidized-bed gasification, have been applied to estimate the relative contribution in the balance equations, in particular the elutriation losses. These become successively more important as the gas velocity is increased, the temperature is decreased and/or the feed size is decreased. An important finding of the simulations is that, for the conditions of practical interest, a quasi-steady approximation can be made for the behavior of fine particles with respect to the class of mother particles.

A mixed numerical (mother class) and analytical (fine class) solution of the quasi-steady population balance equations is incorporated in a model for a bubbling fluidized bed biomass gasifier schematized according to the two-phase theory of fluidization, where the emulsion phase is assumed to be perfectly mixed and a plug-flow approximation is used for the bubble phase and the splash and freeboard zones. The coupled particle population balance and the fluidized bed models are used to simulate gasification of wood with air at a laboratory scale. Simulations made for the typical conditions of the experiments and by varying the equivalent ratio and the bed temperature show good agreement with the measurements for the gas composition (and LHV) and the tar content of the gas.

Although the model presented in this study represents a significant advancement with respect to the current state of the art, there are still numerous aspects that deserve further developments. These include the formulation of more accurate sub-models for the processes of particle size reduction (primary and secondary fragmentation, abrasion) and the experimental determination of the limit particle size between mother and fine classes. Extensive experimental investigation, which can provide detailed information on the particle size distribution on dependence on the operating conditions, is also highly desirable not only for an improved understanding of the process but also for the experimental validation of the model proposed. The mathematical model should be improved with a more accurate description of the reaction rates with the assumption of regimes that should vary, for instance, on dependence of the combustion or the gasification process. Also, effects associated with non-isothermal behavior may be important and should be properly taken into account.

Nomenclature

A	pre-exponential factor [s^{-1}]
c	species concentration [kmol m^{-3}]
d	particle diameter [m]
d_f	boundary diameter between the class of fine and mother particles [m]
d_{max}	maximum particle diameter [m]
d_{min}	minimum diameter for 99.5% of feed particles [m]
D	diffusivity [m^2 s^{-1}]
D	bed diameter [m]
E	activation energy [J $kmol^{-1}$]
ER	equivalent ratio
F_0	wood feed rate [kg s^{-1}]
g	acceleration of gravity [m s^{-2}]
K_a	abrasion constant
K_f	fragmentation constant
H_B	expanded bed height [m]
LHV	gas low heating value [J m^{-3}]
M	molecular weight [kg $kmol^{-1}$]
P	particle size distribution [kg m^{-1}]
R_g	Universal gas constant [J $kmol^{-1}$ K^{-1}]
S	area of reactor cross section [m^2]
T	temperature [K]
t	time [s]
u	velocity [m s^{-1}]
z	spatial coordinate [m]
W_I	sand mass [kg]
X	molar fraction
Y	mass fraction

Greek symbols

ε	void fraction
μ	mean value of the input fractional size distribution [m]
μ_g	viscosity [Pa s]
ν	stoichiometric coefficients for biomass primary pyrolysis
ν^*	stoichiometric coefficients for thermal cracking of primary tar
ρ	density [kg m^{-3}]
σ	standard deviation of the input fractional size distribution
φ	sand sphericity
Π	pressure [Pa]

Superscripts

e	Emulsion phase
0	Input conditions

b	Bubble phase
SF	Splash and freeboard

Subscripts

b1	char oxidation
b2	char gasification (CO_2)
b3	char gasification (H_2O)
c1	primary tar combustion
c2	CH_4 combustion
c3	CO combustion
c4	H_2 combustion
c5	refractory tar combustion
c	char
E	equilibrium
F	fine particles
g	gas phase
M	mother particles
mf	minimum fluidization conditions
S	solid phase
SF	splash and freeboard zone
wg	water gas shift

REFERENCES

[1] Beenackers AACM, Maniatis K. Gasification technologies for heat and power from biomass. In: Chartier P, Ferrero GL, Henius UM, Hultberg J, Sachau J, Wiinblad M, editors. Proceedings of the 9th European Bioenergy Conference. New York: Pergamon Press; 1996. pp. 228–59.

[2] Hamel S, Krumm W. Mathematical modeling and simulation of bubbling fluidized bed gasifiers. Powder Technol 2001;120(1):105–12.

[3] Raman P, Walawender WP, Fan LT, Chang CC. Mathematical model for the fluid-bed gasification of biomass materials. Application to feedlot manure. Ind Eng Chem Process Des Dev 1981;20(4):686–92.

[4] Jiang H, Morey RV. A numerical model of a fluidized bed biomass gasifier. Biomass Bioenergy 1992;3(6):431–47.

[5] Bilodeau JF, Therien N, Proulx P, Czernik S, Chornet E. A mathematical model of fluidized bed biomass gasification. Can J Chem Eng 1993;71(4):549–57.

[6] Fiaschi D, Michelini M. A two-phase one-dimensional biomass gasification kinetics model. Biomass Bioenergy 2001;21(2):121–32.

[7] Sadaka SS, Ghaly AE, Sabbah MA. Two-phase biomass air-steam gasification model for fluidized bed reactors: Part I – model development. Biomass Bioenergy 2002;22(6):439–62.

[8] Sadaka SS, Ghaly AE, Sabbah MA. Two-phase biomass air-steam gasification model for fluidized bed reactors: Part II – model sensitivity. Biomass Bioenergy 2002;22(6):463–77.

[9] Sadaka SS, Ghaly AE, Sabbah MA. Two-phase biomass air-steam gasification model for fluidized bed reactors: Part III – model validation. Biomass Bioenergy 2002;22(6):479–83.

[10] Radmanesh R, Chaouki J, Guy C. Biomass gasification in a bubbling fluidized bed reactor: experiments and modeling. AIChE J 2006;52(12):4258–72.

[11] Kaushal P, Abedi J, Mahinpey N. A comprehensive mathematical model for biomass gasification in a bubbling fluidized bed reactor. Fuel 2010;89(12):3650–61.

[12] Kaushal P, Proell T, Hofbauer H. Application of a detailed mathematical model to the gasifier unit of the dual fluidized bed gasification plant. Biomass Bioenergy 2011;35(7):2491–8.

[13] Levenspiel O, Kunii D, Fitzgerald T. The processing of solids of changing size in bubbling fluidized beds. Powder Technol 1968/69;2(2):87–96.

[14] Chen TP, Saxena SC. A mechanistic model applicable to coal combustion in fluidized beds. AIChE Symp Series 1978;74(176):149–61.

[15] Weimer AW, Clough DE. Dynamics of particle size/conversion distribution in fluidized beds: application to char gasification. Powder Technol 1980;26(1):11–6.

[16] Overtuf BW, Reklaitis GV. Fluidized-bed reactor model with generalized particle balances. AIChE J 1983;29(5):813–20.

[17] Ray YC, Jiang TS, Jiang TL. Particle population model for a fluidized bed with attrition. Powder Technol 1987;52(1):35–48.

[18] Wang Q, Luo Z, Ni M, Cen K. Particle population balance model for a circulating fluidized bed boiler. Chem Eng J 2003;93(2):121–33.

[19] Saastamoinen JJ, Tourunen A, Hämäläinen J, Hyppänen T, Loschkin M, Kettunen A. Analytical solutions for steady and unsteady state particle size distributions in FBC and CFBC boilers for non-breaking char particles. Combust Flame 2003;132(3):395–405.

[20] Khan AA, De Jong W, Gort DR, Spliethoff H. A fluidized bed biomass combustion model with discretized population balance 1. Sensitivity analysis. Energy Fuels 2007;21(4):2346–56.

[21] Khan AA, De Jong W, Gort DR, Spliethoff H. A fluidized bed biomass combustion model with discretized population balance 2. Experimental studies and model validation. Energy Fuels 2007;21(6):3709–17.

[22] Saastamoinen J, Pikkarainen T, Tourunen A, Räsänen M, Jäntti T. Model of fragmentation of limestone particles during thermal shock and calcination in fluidised beds. Powder Technol 2008;187(3):244–51.

[23] Pis JJ, Fuertes AB, Artos V, Suarez A, Rubiera F. Attrition of coal ash particles in a fluidized bed. Powder Technol 1991;66(1):41–6.

[24] Davidson JF, Harrison D. Fluidized particles. New York: Cambridge University Press; 1963.

[25] Di Blasi C. Modeling chemical and physical processes of wood and biomass pyrolysis. Prog Energy Combust Sci 2008;34(1):47–90.

[26] Di Blasi C. Combustion and gasification rates of lignocellulosic chars. Progr Energy Combust Sci 2009;35(2):121–40.

[27] Lede J. The cyclone: a multifunctional reactor for the fast pyrolysis of biomass. Ind Eng Chem Res 2000;39(4):893–903.

[28] Rath J, Staudinger G. Cracking reactions of tar from pyrolysis of spruce wood. Fuel 2001;80(10):1379–89.

[29] Boroson ML, Howard JB, Longwell JP, Peters AW. Products yields and kinetics from the vapor phase cracking of wood pyrolysis tars. AIChE J 1989;35(1):120–8.

[30] Di Blasi C. Dynamic behavior of stratified downdraft gasifiers. Chem Eng Sci 2000;55(15):2931–44.

[31] Di Blasi C. Modeling wood gasification in a countercurrent fixed-bed reactor. AIChE J 2004;50(9):2306–19.

[32] Saastamoinen J, Tourunen A. Model for char combustion, particle size distribution, and inventory in air and oxy-fuel combustion in fluidized beds. Energy Fuels 2012;26(1):407–16.

[33] Mandl C, Obernberger I, Biederman F. Modeling of an updraft fixed-bed gasifier operated with softwood pellets. Fuel 2010;89(12):3795–806.

[34] Di Blasi C, Branca C. Modeling a stratified downdraft wood gasifier with primary and secondary air entry. Fuel 2013;104:847–60.

[35] Gerber S, Behrendt F, Oevermann M. An Eulerian modeling approach of wood gasification in a bubbling fluidized bed reactor using char as bed material. Fuel 2010;89(10):2903–17.

[36] Ranz WE, Marshall WR. Evaporation from drops. Chem Eng Prog 1952;48(3):141–6.
[37] Kashiwagi T, Nambu H. Global kinetic constants for thermal oxidative degradation of a cellulosic sample. Combust Flame 1992;88(3-4):345–68.
[38] Barrio M, Gobel B, Risnes H, Henriksen U, Hustad JE, Sørensen LH. Steam gasification of wood char and the effect of hydrogen inhibition on the chemical kinetics. In: Bridgwater AV, editor. Progress in thermochemical biomass conversion. Oxford: Blackwell Science Ltd.; 2001. pp. 32–46.
[39] Barrio M, Hustad JE. CO_2 gasification of birch char and the effect of CO inhibition on the calculation of chemical kinetics. In: Bridgwater AV, editor. Progress in thermochemical biomass conversion. Oxford: Blackwell Science Ltd.; 2001. pp. 47–60.
[40] Bryden KM, Ragland K. Numerical modeling of a deep, fixed-bed combustor. Energy Fuels 1996;10(2):269–75.
[41] Cooper J, Hallet WL. A numerical model for packed-bed combustion of char particles. Chem Eng Sci 2000;55(20):4451–60.
[42] Yan H, Heidenreich C, Zhang D. Mathematical modelling of a bubbling fuidised-bed coal gasifier and the significance of 'net flow'. Fuel 1998;77(9–10):1067–79.
[43] Biba V, Macak J, Klose E, Malecha J. Mathematical model for the gasification of coal under pressure. Ind Eng Prod Res Dev 1978;17(1):92–8.
[44] Karim GA, Mohindra D. A kinetic investigation of the water–gas shift reaction in homogeneous systems. J Inst Fuel 1974;47:219–23.
[45] Yoon H, Wei J, Denn MM. A model for moving bed coal gasification reactors. AIChE J 1978;24(5):885–903.
[46] Kunii D, Levenspiel O. Fluidization engineering. 2nd ed. Stoneham, MA: Butterworth-Heinemann; 1991.
[47] Mori S, Wen CY. Estimation of bubble diameter in gaseous fluidized beds. AIChE J 1975;21(1):109–15.
[48] Clift R, Grace JR. In: Davidson JF, et al., editors. Fluidization. 2nd ed. New York: Academic Press; 1985.
[49] Purnomo Aerts DJ, Ragland KW. Pressurized downdraft combustion of wood chips. In: Proceeding of the 23rd Symposium (Int.) on Combustion. Pittsburgh: The Combustion Institute; 1990. pp. 1025–32.
[50] Perry RH, Green DW, Maloney JO, editors. Perry's chemical Engineers' handbook. 6th ed. New York: McGraw-Hill; 1984.
[51] Di Blasi C. Influences of model assumptions on the predictions of cellulose pyrolysis in the heat transfer controlled regime. Fuel 1996;75(1):58–66.
[52] Di Blasi C. Multi-phase moisture transfer in the high-temperature drying of wood particles. Chem Eng Sci 1998;53(353):353–66.
[53] Di Blasi C. Physico-chemical processes occurring inside a degrading two-dimensional anisotropic porous medium. Int J Heat Mass Transfer 1998;41(24):4139–50.
[54] Di Blasi C. Modelling intra- and extra-particle processes of wood fast pyrolysis. AIChE J 2002;48(10):2386–97.
[55] Santaniello R, Galgano A, Di Blasi C. Coupling transport phenomena and secondary reactions in the modeling of microwave-induced pyrolysis of wood. Fuel 2012;96:355–73.
[56] Halder PK, Basu P. Attrition of spherical electrode carbon particles during combustion in a turbulent fluidized bed. Chem Eng Sci 1992;47(3):527–32.
[57] Colakyan M, Levenspiel O. Elutriation from fluidized bed. Powder Technol 1984;38(3):223–32.
[58] Haider A, Levenspiel O. Drag coefficient and terminal velocity of spherical and nonspherical particles. Powder Technol 1989;58(1):63–70.
[59] Yanenko NN. The method of fractional steps. New York: Springer-Verlag; 1971.
[60] Boris JP, Book DL. Flux-Corrected Transport III. Minimal-error FCT Algorithms. J Comp Phys 1976;20(4):397–431.
[61] Gogolek PEG, Grace JR. Fundamental hydrodynamics related to pressurized fluidized bed combustion. Prog Energy Combust Sci 1995;21(5):419–51.
[62] Frossling N. Uber die verdunstung fallender tropfen (The evaporating of falling drops). Gerlands Beitrage zur Geophysik 1938;52:170–216.
[63] La Nauze RD, Jung K. The kinetics of combustion of petroleum coke particles in a fluidized-bed combustor, 19th Symposium (Int.) on Combustion. Pittsburgh: The Combustion Institute; 1982. pp. 1087–92.
[64] Prins W, Casteleijn TP, Draijer W, van Swaaij WPM. Mass transfer from a freely moving single sphere to the dense phase of a gas fluidized bed of inert particles. Chem Eng Sci 1985;40(3):481–97.
[65] Yang YB, Sharifi VN, Swithenbank J, Ma L, Darvell LI, Jones JM, Porkashanian M, Williams A. Combustion of a single particle of biomass. Energy Fuels 2008;22(1):306–16.
[66] Narvaez I, Orio A, Aznar MP, Corella J. Biomass gasification with air in an atmospheric bubbling fluidized bed. Effect of six operational variables on the quality of the produced raw gas. Ind Eng Chem Res 1996;35(7):2110–20.
[67] Buekens AG, Schoeters GJ. Modeling of biomass gasification. In: Overend RP, Milne TA, Mudge LK, editors. Fundamentals of thermochemical biomass conversion. London: Elsevier; 1985. pp. 619–90.